Paths of Shear-mode Cracks in Ferritic and Austenitic Steel

T. Vojtek and J. Pokluda

Brno University of Technology, Faculty of Mechanical Engineering, Technická 2, 616 69 Brno, Czech Republic, e-mail: vojtek4@seznam.cz

ABSTRACT. *This work is focused on experimental study of shear crack paths in ferritic steel and austenitic steel. The aim is to elucidate the growth micromechanism of mode II and III cracks. The crack path and the surface topography were studied by means of 3D reconstruction of the fracture surfaces using stereophotogrammetry in SEM. Measurements by means of the profile analysis were used to determine local deflection and twisting angles of the crack with respect to the remote shear direction. The related tendency to mode I crack branching was found to be much higher in austenite than in ferrite. The mean branch deflection of remote mode II cracks in the austenite was close to the theoretical critical angle* $\alpha_{cII} \approx 70°$*. For mode III cracks, the mean twist angle of branches was apparently lower than the critical angle* $\alpha_{cIII} \approx 45°$ *which seems to be associated with the geometrically more difficult branching in mode III with respect to mode II.*

INTRODUCTION

From the point of view of continuum mechanics, the mode II and mode III crack growth rates and the related thresholds $\Delta K_{II,th}$ ($\Delta K_{III,th}$) were expected to be equal [1]. However, there are many indications that this assumption is not sufficiently fulfilled (e.g. [2 - 6]). The problem lies in the fact that, unlike for material elements separated from the crack front, the damage of mode II and mode III elements directly connected with the crack front is asymmetric with respect to both the shear-mode loading and the crack propagation direction. Therefore, the environmentally-assisted incomplete recovery of freshly created fracture surfaces at the crack front can promote the crack propagation only under mode II loading [5, 6].

Mode II and mode III crack paths in the notched specimens can also significantly differ especially in the near-threshold regime (e.g. [7 - 9]). This is caused by a competition between shear and opening modes that can lead to mode I branches. A smooth long crack under a pure in-plane shear can get a maximum support of mode I loading ($\Delta K_I \approx 1.15\ \Delta K_{II}$) by deflection of the shear plane to planes close to $\alpha_{cII} \approx 70°$ (e.g. [7, 10]). A necessary condition for growth of a mode I branch at the mode II crack front was formulated as: the branch crack stress intensity range, ΔK_I, must be greater than the threshold $\Delta K_{I,th}$ [11]. The formation of the mode I segments corresponds to a rotation around the axis parallel to the crack front which is relatively easy: the tilt plane intersects the main crack plane along the line (curve). On the other hand, the mode III

crack segments under a pure remote shear can get an additional mode I support only by twisting around the axis perpendicular to the crack front, e.g., [7, 12]. The condition for mode I branching is, in principle, equal to that for mode II loaded crack. Here, however, $\Delta K_I = \Delta K_{III}$ and the twist angle $\alpha_{cIII} = 45°$. Since the plane of the twisted element and that of the main crack intersect just in one point, the twisting can occur only on microscopic ledges at the main crack front. Therefore, the size of the twisted elements becomes rather limited. Thus, in the pure shear case, the formation of extended mode I branches at the mode II crack front is much easier than that at the front of mode III cracks. These are, most probably, the reasons why the crack growth rate in mode III was often found to be lower than that in mode II (e.g., [2, 5]. In the case of torsion loading, however, the mode III cracks can get some mode I support just by a deflection of the maximum shear plane. This is the reason why the near-threshold, semi-elliptical II+III microcracks in notched specimens under torsion often propagate along planes deflected of the maximum shear plane [6]. Such an initial mixed-mode shear growth is often stopped by a formation of mode I branches leading to the factory-roof fracture morphology (e.g., [12, 13]).

The aim of this study is to find and describe microscopic crack paths in ferrite and austenite to elucidate crack growth mechanisms under shear modes II and III. The crack path and the surface topography were studied by means of 3D reconstruction of the fracture surfaces using stereophotogrammetry.

EXPERIMENTS

The first experiment was done on cylindrical bars with circumferential cracked notch that were loaded in different combinations of modes II and III as a function of the angle φ (see Fig. 1). On the top and bottom of the circle the crack was loaded in a pure mode II, on the left and right margin by pure mode III and, in between, by a mixed-mode II+III. Stress intensity factors (SIFs) in mode II and III were numerically calculated using FEM. The exact central point of the bar the bending moment is zero (Fig. 2). Pre-cracks were created by compressive cyclic loading in mode I to obtain smooth fracture surfaces. After the experiment, the specimens were fractured under very low temperature or by cyclic tensile loading. The second experiment was cyclic torsion (mode III) and the third one was shear loading of CTS specimens (mode II).

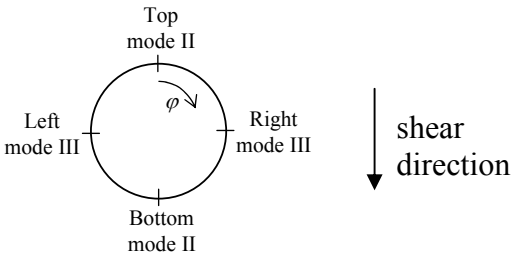

Figure 1. Cross section of the shear specimen with the corresponding loading modes.

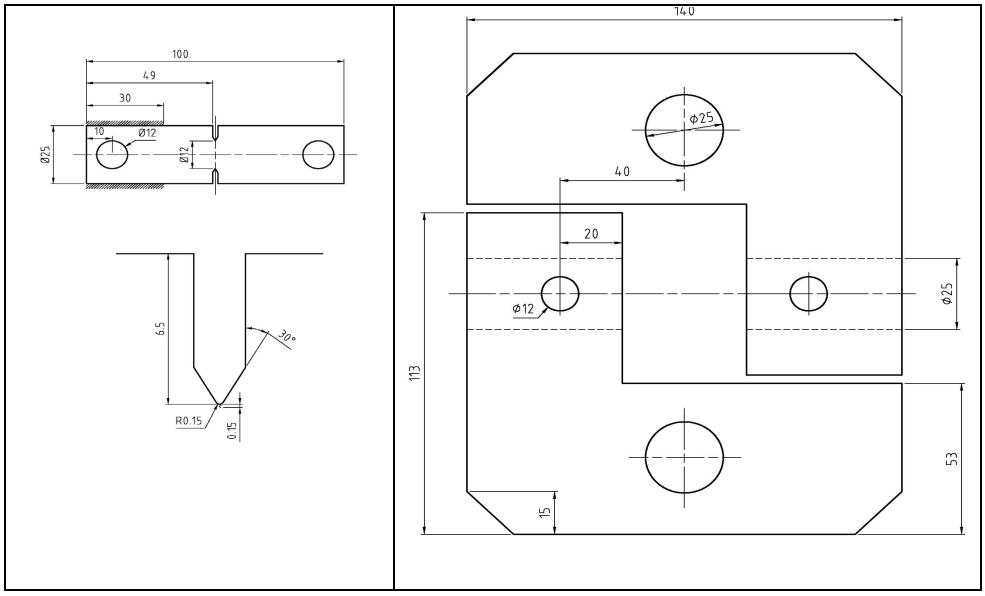

Figure 2. Scheme of the experiment with cylindrical specimens loaded in a pure shear.

EXPERIMENTAL RESULTS

Three crack path regions are depicted on each part of Fig. 3 that shows fracture morphologies of both the ferrite and austenite: a precrack emanating from the notch, a shear crack and the final fracture (brittle or fatigue fracture in mode I).

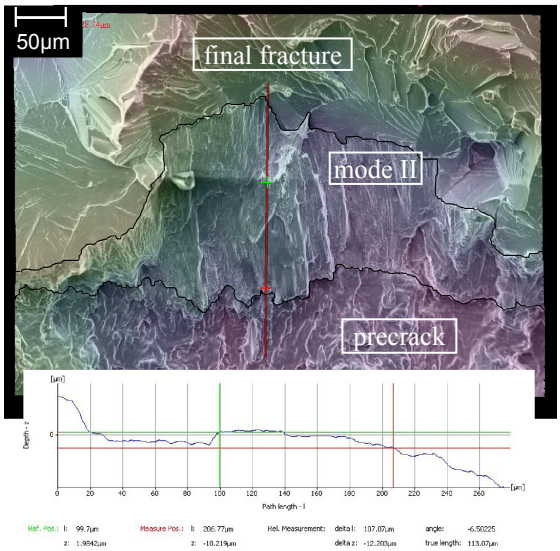

a) mode II in ferrite

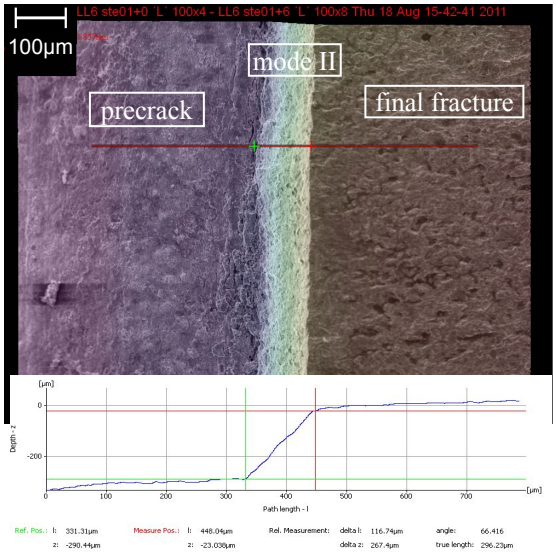

b) mode II in austenite

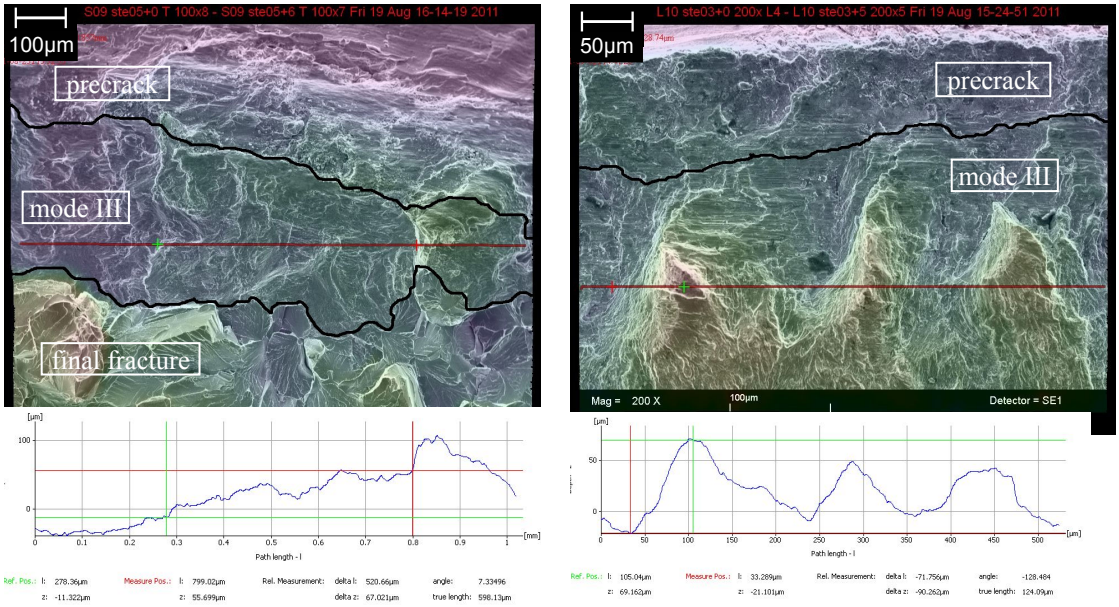

c) mode III in ferrite d) mode III in austenite

Figure 3. Comparison of crack paths in mode II and III in ferrite and austenite.

Profile analysis was carried out after the 3D reconstruction of fracture surfaces. The profile is determined by a cutting plane denoted by the red line in Fig 3. The coordinate l passes along the red line from left to right or from top to bottom. Two points on the profile are marked by green and red cross. These points are used for angle measuring. The profile line direction is either parallel to shear (deviation angle is α) or perpendicular to shear (deviation angle is β). Under each shear mode II or III the crack deflects and twists in a different way, which is described by the angles $\alpha_{II,III}$ and $\beta_{II,III}$.

Table 1. Deflection and twisting angles [°]

mode	angle	branch type	material	Specimen	
				shear	CTS/Torsion
II	α_{II}	deflection	ferrite	**18 ± 17**	**19 ± 8**
			austenite	**66 ± 4**	
	β_{II}	twisting	ferrite	**18 ± 16**	**25 ± 20**
			austenite	**7 ± 8**	
III	α_{III}	twisting	ferrite	**19 ± 13**	**13 ± 10**
			austenite	**33 ± 23**	
	β_{III}	deflection	ferrite	**18 ± 13**	**33 ± 34**
			austenite	**19 ± 14**	

Deflection and twisting angles were measured on SEM stereo images for each mode and specimen type. They are presented in Table 1 as the mean value $\overline{\alpha} = \frac{1}{n}\sum_i \alpha_i$ and standard deviation $s_\alpha = [1/(n-1)\sum_i (\alpha_i - \overline{\alpha})]^{1/2}$. Frequencies of each angle range are presented in the histograms in Fig. 4 where the angles α and β, loading mode (II or III) and specimen type are distinguished.

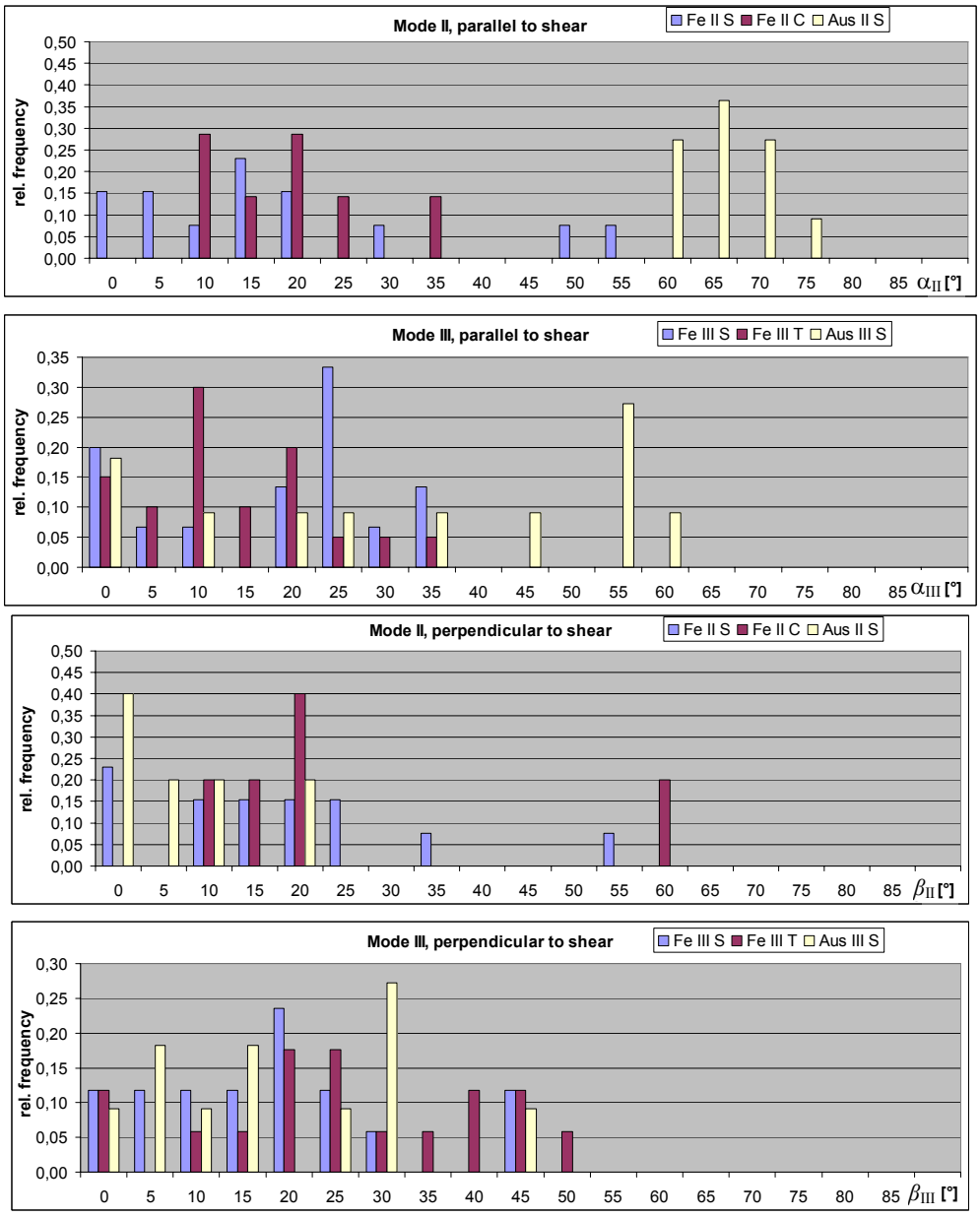

Figure 4. Frequencies of crack deviation angles with respect to the shear plane.

Data obtained in the ferritic steel are denoted as “Fe II S” and “Fe III S” for cylindrical specimens, “Fe II C” for CTS specimens loaded by a pure shear and “Fe III T” for cylindrical specimens loaded by torsion. Data corresponding to the austenitic cylindrical specimens loaded by a pure shear are denoted as “Aus II S”.

The following Figs 5a – 5f show examples of the shear crack morphologies in ferrite and austenite. There are two apparent differences between these two materials. First, in austenite the tendency to mode I branching was found to be much higher than that in ferrite and the crack growth is homogeneous along the precrack front. Second, fibrous patterns were found in each facet in ferrite. Different orientations of these patterns indicate a crystallography-controlled crack growth. In austenite no such patterns were detected which implies no crystallography influence.

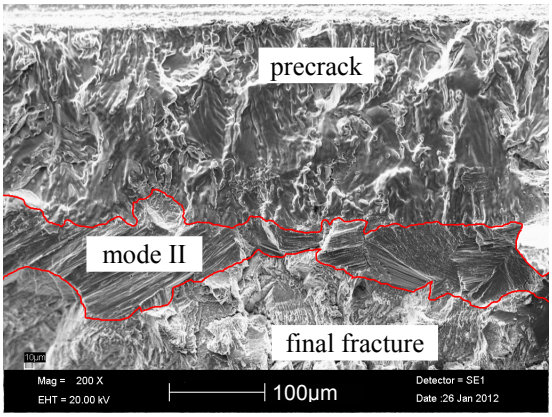

a) ferrite, mode II, CTS

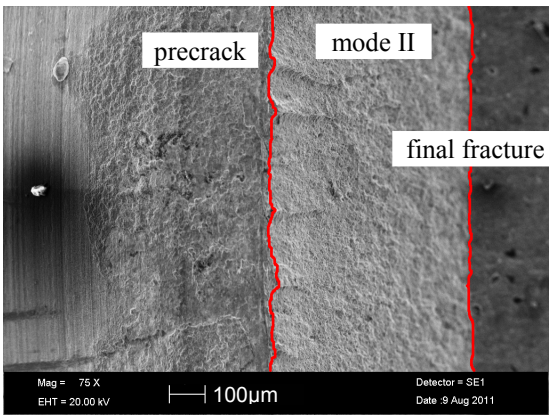

b) austenite, mode II, shear

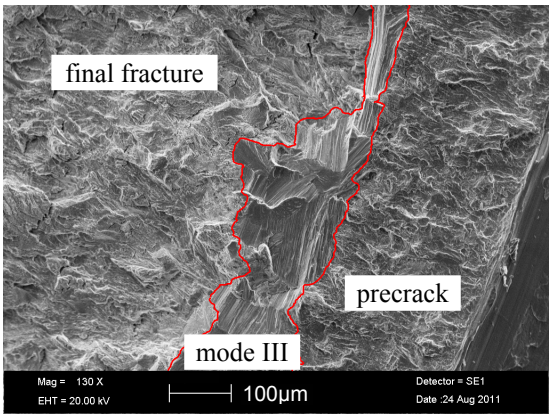

c) ferrite, mode III, torsion

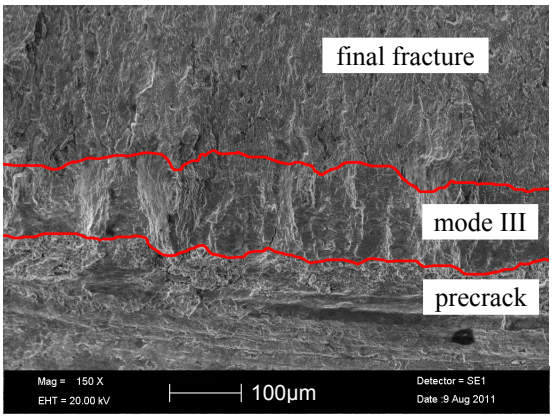

d) austenite, mode III, shear

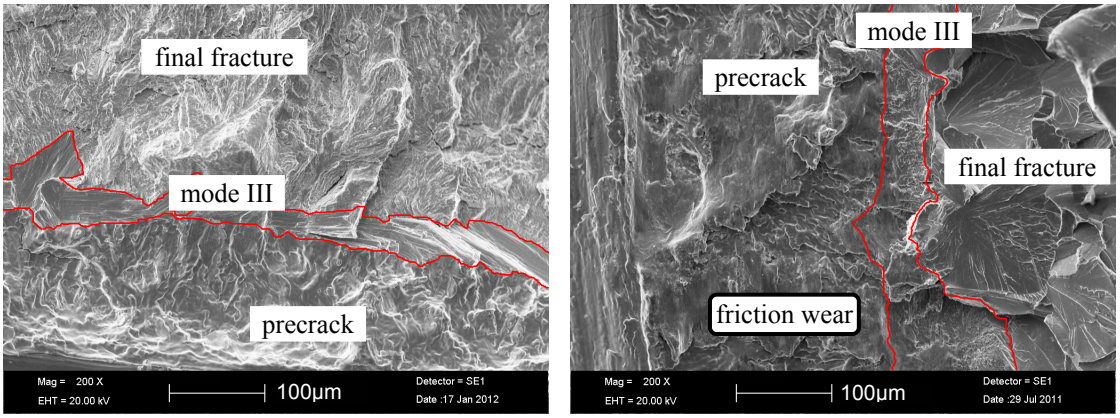

e) ferrite, mode III, shear (low ΔK) f) ferrite, mode III, shear (high ΔK)

Figure 5. Shear crack morphologies in ferrite and austenite.

Under shear mode loading, the crack flanks mostly experience a rubbing action. However, when low, near-threshold loadings are applied, no visible friction traces were observed (Fig. 5e). Frictional wear was evident only when loads as high as $\Delta K > 2\Delta K_{th}$ were applied (Fig. 5f).

DISCUSSION

The crack morphologies revealed that the shear cracks in austenite had a much higher tendency to deflection and twisting to form mode I branches than those in ferrite. In order to explain that effect, one can use the above mentioned criteria for crack branching of mode II and mode III cracks. The threshold values for ferrite are $\Delta K_{\mathrm{I,th}} = 2.7$ MPam$^{1/2}$, $\Delta K_{\mathrm{II,th}} = 1.6$ MPam$^{1/2}$, $\Delta K_{\mathrm{III,th}} = 2.6$ MPam$^{1/2}$ and for austenite $\Delta K_{\mathrm{I,th}} = 2.2$ MPam$^{1/2}$, $\Delta K_{\mathrm{II,th}} = 2.3$ MPam$^{1/2}$, $\Delta K_{\mathrm{III,th}} = 4.7$ MPam$^{1/2}$ [14 - 16]. For mode II, the criterion gives $1.15 \times \Delta K_{II\,th} > \Delta K_{I\,th}$. Consequently, the criterion shows $2.6 > 2.2$ for austenite (branching) but $1.8 < 2.7$ for ferrite (no branching). For mode III, the criterion gives $\Delta K_{III\,th} > \Delta K_{I\,th}$ and, similarly, $4.7 > 2.2$ for austenite (branching) but $2.6 < 2.70$ for ferrite (no branching). Note that the mean deflection angle in austenite $\alpha_{\mathrm{II}} \approx 66°$ is close to $\alpha_{\mathrm{cII}} \approx 70°$. On the other hand, the mean twist angle $\alpha_{\mathrm{III}} \approx 33°$ is apparently less than $\alpha_{\mathrm{cIII}} \approx 45°$. This is, most probably, associated with the geometrically more difficult branching process in mode III with respect to mode II.

CONCLUSIONS

Fracture surfaces of specimens from ferritic and austenitic steel were analysed after near-threshold fatigue failure by shear-mode fatigue loading. The main results can be

summarized as follows:

1. Fracture surface morphologies in austenite and ferrite are significantly different. In particular, the tendency to mode I branching in the austenite is higher than that of the ferrite. Unlike in the austenite, diversely oriented fibrous patterns were observed on each facet in the ferrite.
2. Unlike in ferrite, simple LEFM criteria for mode I branching were found to be fulfilled in austenite. This elucidates the higher tendency to form mode I branches in the latter material where the mean branch deflection $\alpha_{II} \approx 66°$ of the remote mode II cracks is close to the theoretical critical angle $\alpha_{cII} \approx 70°$. For the remote mode III cracks, the mean twist angle $\alpha_{III} \approx 33°$ of branches was apparently lower than the critical angle $\alpha_{cIII} \approx 45°$. This seems to be associated with the geometrically more difficult branching in mode III with respect to mode II.

ACKNOWLEDGEMENTS

This work was supported by the Czech Science Foundation in the frame of the project No. P108/10/0698. The authors thank to Prof. R. Pippan and Dr. A. Hohenwarter from the Erich Schmid Institute of Materials Science in Leoben, Austria, for their help.

REFERENCES

1. Murakami Y., Kusumoto R., Takahashi K. (2002) in *Fracture Mechanics beyond 2000*, Neimitz A. et al. (eds), EMAS, Sheffield, pp. 493-500.
2. Nayeb-Hashemi, H., McClintock, F.A., Ritchie, R.O. (1983) *Int. J. Fracture* **23,** 163–185.
3. James M., Herman D. J., Scott F. (2003). In: *Fatigue and Fracture Mechanics*, Daniewitz S. R., Newman J. C., Schwalbe K. H. (Eds)., ASTM, West Conshohocken.
4. Schöllmann M., Fulland M., Richard H.A. (2003) *Engng Fract. Mechanics* **70** 249–268.
5. Pokluda, J., Tratting, G., Martinschitz, C., Pippan, G. (2008) *Int. J. Fatigue* **30,** 1498-1506.
6. Pokluda, J., Pippan, R. (2005) *Fat. Fract. Engng. Mater. Structures* **28,**179-185.
7. Pook L. P. (2002) *Crack Paths*, Wit Press, Southampton-Boston.
8. Suresh S. (1998) *Fatigue of Materials*, Cambridge University Press.
9. Pokluda J., Šandera P. (2010) *Micromechanisms of Fracture and Fatigue,* Springer.
10. Murakami, Y. (2002) *Metal Fatigue: Effects of Small Defects and Nonmetallic Inclusions*, Elsevier.
11. Pook L. P., Greenan A. F. (1976). In: *Fatigue Testing and Design,* Vol. 2, pp.30.1 – 30.33, Buntingford, Herts
12. Pokluda J., Slámečka K. a Šandera P. (2010) *Engng Fract. Mechanics* **77,** 1763 – 1771.
13. Tscheg E. K., Stanzel S. E. (1988). In: *Basic Questions in Fatigue, Vol.1,* ASTM STP 924, Vol. 1, pp. 214 - 232, Philadelphia.
14. Pippan R. (1991) Mater. Sci. Eng. A, **138,** 1 – 13.
15. Pokluda J., Kondo Y., Slámečka K., Šandera P. a Horníková J. (2008) *Key Engng. Materials* **385-387,** 49 - 52.
16. Vojtek T., Pokluda J., Hohenwarter A, Pippan R. (2012). In: European Conference on Fracture (ECF19), Kazan (submitted).